

# Reanalysis-based Global Radiative Response to Sea Surface Temperature Patterns: Evaluating the Ai2 Climate Emulator

Senne Van Loon, Maria Rugenstein, & Elizabeth A. Barnes

Department of Atmospheric Science, Colorado State University, Fort Collins, Colorado, USA

## Key Points:

- AI emulator of ERA5 produces physically consistent sensitivity of global-mean radiation to local sea surface temperature (SST) perturbations
- Reconstruction of global-mean top-of-atmosphere radiation from historical SST anomalies fails to capture the expected negative trend
- SST-patch forcing experiments can evaluate climate emulators in an idealized setting, tracing physical relationships between variables

arXiv:2502.10893v1 [physics.ao-ph] 15 Feb 2025

---

Corresponding author: Senne Van Loon, [senne.van\\_loon@colostate.edu](mailto:senne.van_loon@colostate.edu)

## Abstract

The sensitivity of the radiative flux at the top of the atmosphere to surface temperature perturbations cannot be directly observed. The relationship between sea surface temperature and top-of-atmosphere radiation can be estimated with Green’s function simulations by locally perturbing the sea surface temperature boundary conditions in atmospheric climate models. We perform such simulations with the Ai2 Climate Emulator (ACE), a machine learning-based emulator trained on ERA5 reanalysis data (ACE2-ERA5). This produces a sensitivity map of the top-of-atmosphere radiative response to surface warming that aligns with our physical understanding of radiative feedbacks. However, ACE2-ERA5 likely underestimates the radiative response to historical warming. We argue that Green’s function experiments can be used to evaluate the performance and limitations of machine learning-based climate emulators by examining if causal physical relationships are correctly represented and testing their capability for out-of-distribution predictions.

## Plain Language Summary

At the top of the atmosphere, the Earth’s energy budget is determined by the balance between incoming and outgoing radiation. This balance is influenced by the surface temperature. The exact relationship between the two is not directly observable. Here, we estimate this relationship by utilizing a machine learning model (ACE2-ERA5) that was trained to replicate the Earth’s atmosphere based on data from ERA5, a dataset that combines model predictions with observations to create a coherent picture of the climate evolution since 1940. By performing idealized experiments, we find that ACE2-ERA5 can produce a physically consistent relationship between surface temperature and the top-of-atmosphere radiation. These idealized experiments can be used to evaluate the performance of machine learning models in climate science, by testing if they correctly represent the physical relationships between variables and if they can make predictions outside of the range of their training data. Although these results are promising, ACE2-ERA5 does not succeed in predicting the top-of-atmosphere radiation based on historical warming. The idealized simulations offer a way to systematically test machine learning-based climate emulators and indicate that the emulators might need energy conservation to produce reliable predictions.

## 1 Introduction

### 1.1 Motivation

Understanding how the atmosphere responds to forcing is one of the most fundamental questions in climate science. To answer this question, we currently depend on general circulation models (GCMs) to correctly model the physics of the coupled ocean-atmosphere system. To date, GCMs are the best tools we have to study the climate system on long timescales, and over the course of decades we have developed an understanding of which problems can or cannot be addressed with this tool (Randall et al., 2018). For example, GCMs have given us the ability to constrain future projections for many atmospheric variables, such as global-mean surface temperature, and have helped to attribute and understand human influences on the climate (Flato et al., 2013; IPCC, 2021). However, these GCMs are generally computationally expensive and rely on parametrizations to represent sub-grid-scale processes and radiative effects, which can lead to biases compared to observations (e.g., Soden et al., 2018; Forster et al., 2021). For instance, GCMs struggle to correctly simulate cloud processes and fail to reproduce the observed patterns of surface warming and precipitation (e.g., Xiang et al., 2017; Seager et al., 2019; Wills et al., 2022; Rugenstein, Dhame, et al., 2023; Zheng et al., 2023).

Recent advances in machine learning (ML) have made it possible to emulate the physical processes in the atmosphere in a computationally efficient way (e.g., Watt-Meyer et al., 2023; Kochkov et al., 2024; Guan et al., 2024; Cachay et al., 2024; Cresswell-Clay et al., 2024;

Watt-Meyer et al., 2024). These emulators replace parts or the entirety of the traditional GCMs with deep learning methods by extracting the relevant physical relationships from observational products or other climate models. The progress made over the last few years has been significant and machine learning is showing great promise to address many open problems in climate science (Eyring et al., 2024; Bracco et al., 2025). Yet, these ML-based emulators have to be evaluated before they can be trusted to answer actual scientific questions similar to traditional GCMs (Ullrich et al., 2025).

Evaluating ML climate emulators can go hand-in-hand with increasing our scientific understanding of the climate system. Thus, the purpose of this work is twofold: (1) to evaluate the response of the top-of-atmosphere (ToA) radiation to sea surface temperature anomalies from reanalysis-based simulations, and (2) to propose a framework in which ML-based climate emulators can be tested in an idealized, yet process-based, setting. To achieve this, we perform atmospheric Green’s function simulations (Bloch-Johnson et al., 2024) with the Ai2 Climate Emulator (ACE, Watt-Meyer et al., 2023; Duncan et al., 2024; Watt-Meyer et al., 2024), and compare the results to physics-based GCMs.

## 1.2 Green’s function experiments with the Ai2 Climate Emulator

In the context of this work, the Green’s function refers to the linear response of the atmosphere to local perturbations of sea surface temperature (Branstator, 1985; Barsugli & Sardeshmukh, 2002; Bloch-Johnson et al., 2024). Computing the Green’s functions requires the simulation of thousands of model years, but, once calculated, can be used to study the response of any simulated variable to any sea surface temperature anomaly with virtually no additional computational expense. Moreover, because the Green’s function portrays a causal response, the resulting sensitivity maps enhance our understanding of the underlying physical mechanisms of the response (e.g., Alessi & Rugenstein, 2023).

In particular, the Green’s function method has been successful in estimating the response of ToA radiation to sea surface temperature anomalies and understanding the varying radiative feedbacks over the historical period (e.g., C. Zhou et al., 2017; Dong et al., 2019). This problem is especially interesting because it directly influences the global energy budget at the top of the atmosphere:  $N = F + R$ , where  $N$  is the net radiative imbalance,  $F$  is the radiative forcing (due to, e.g., CO<sub>2</sub> or aerosol emissions), and  $R$  is the radiative response to surface warming. The radiative imbalance  $N$  is a measure of the excess energy flux into the Earth system ( $N = 0$  in equilibrium) and has been continuously observed by satellites since 2000 (Loeb et al., 2018). To first order,  $R$  is a function of surface temperature, and, in a stable climate, acts as a restoring term for the energy budget. Therefore, knowing how sensitive  $R$  is to varying surface temperature is crucial to understand how much the atmosphere warms in response to a radiative forcing (e.g., Senior & Mitchell, 2000; Andrews et al., 2015, 2022; Rugenstein, Zelinka, et al., 2023).

Importantly, only  $N$  but not  $R$  can be observed. As such, we rely on models to estimate  $R$ . Green’s function simulations are one way of estimating the relationship between the ToA radiation and surface temperature, but – to date – they have always relied on GCMs, and an observation-based relationship has been elusive so far. As mentioned above, GCMs rely on radiative transfer parametrizations to model this relationship, which are known to have biases (Soden et al., 2018). Therefore, there is an ongoing search for alternative tools to evaluate the ToA response to surface warming based on various regression techniques and contrasting models with observations (e.g., Falasca et al., 2025; Rugenstein et al., 2025; Thompson et al., in review; Fredericks, Rugenstein, & Thompson, in prep.; Fredericks, Van Loon, et al., in prep.).

The Ai2 Climate Emulator (ACE) is a data-driven autoregressive model that has been shown to be stable on climatic timescales (Watt-Meyer et al., 2023; Duncan et al., 2024; Watt-Meyer et al., 2024). Version 2 of ACE (ACE2, Watt-Meyer et al., 2024) has been trained on the ERA5 reanalysis dataset (Hersbach et al., 2020), which is based on observa-

tions. When forced with historical sea surface temperature and CO<sub>2</sub> concentrations, ACE2 is able to reproduce the historical data from ERA5 well (see Watt-Meyer et al., 2024). ACE2 can simulate a year in a few minutes of computation time on a single GPU, such that it can be used to perform Green’s function simulations in just a few days (compared to a few weeks for most GCM simulations, depending on the availability of compute nodes).

We give an overview of ACE and its training data in section 2.1. By performing atmospheric Green’s function simulations (section 2.2), we show that the ACE2-ERA5 top-of-atmosphere radiation Green’s function is qualitatively similar to physics-based GCMs (section 3.1). This indicates that ACE2 trained on ERA5 adequately represents the response of the atmosphere to sea surface temperature perturbations and that this relationship is similar in models and observations. However, using the ACE2-ERA5 Green’s function to predict the historical top-of-atmosphere radiative response to surface warming leads to results inconsistent with our knowledge of radiative feedbacks (section 3.2). In section 4, we discuss possible reasons for this discrepancy and explore the use of Green’s function experiments as a systematic test for atmospheric climate emulators.

## 2 Data and Methods

### 2.1 Ai2 Climate Emulator (ACE)

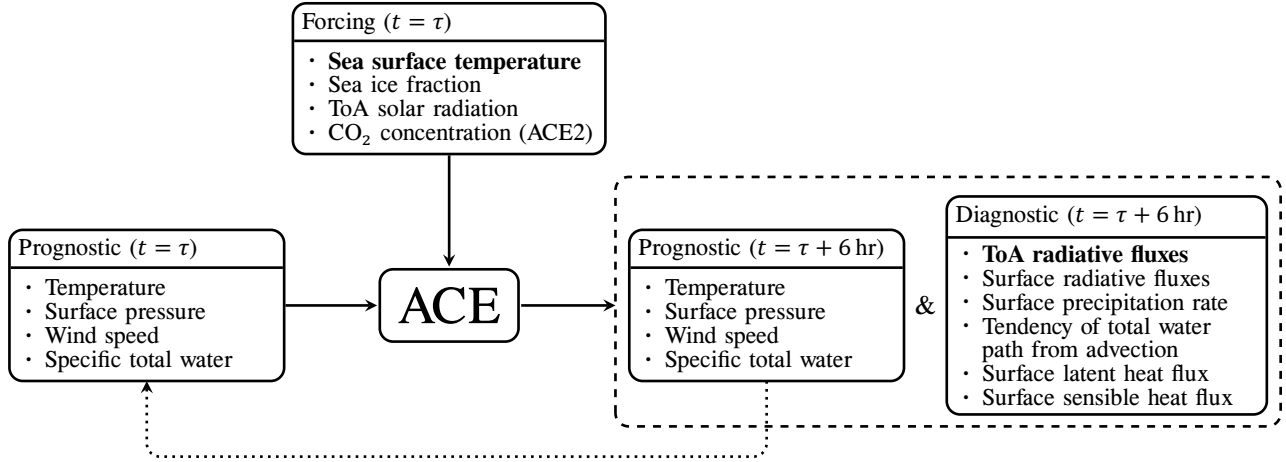
We use three already-trained versions of ACE: ACE-FV3 (Watt-Meyer et al., 2023), ACE-EAM (Duncan et al., 2024), and ACE2-ERA5 (Watt-Meyer et al., 2024), see Supplemental Table S1. ACE is a neural network based on Spherical Fourier Neural Operators (SFNO; Bonev et al., 2023) that is designed to emulate a model of the atmosphere. All three versions of ACE are atmosphere-only autoregressive models that predict the state of the atmosphere at time  $t = \tau + 6$  hr, based on the current state ( $t = \tau$ ) and a forcing that sets the boundary conditions. At every time  $t = \tau$ , ACE uses the forcing climatology (e.g., sea surface temperature) and the prognostic variables (e.g., air temperature) at  $t = \tau$  to predict the state of the atmosphere six hours into the future ( $t = \tau + 6$  hr). The output state at  $t = \tau + 6$  hr includes prognostic variables and diagnostic variables (output only, e.g., radiative fluxes). The prognostic variables at  $t = \tau + 6$  hr, together with the forcing variables, can then be used as input to predict the state at  $t = \tau + 12$  hr, and so on. We found all versions of ACE to be stable for at least four decades, in agreement with Watt-Meyer et al. (2023), Duncan et al. (2024), and Watt-Meyer et al. (2024). All versions of the emulator are forced by ToA incoming solar radiation (rsdt), sea-ice fraction (SIC), and sea surface temperature (SST). ACE2-ERA5 is additionally forced by CO<sub>2</sub> concentration. Fig. 1a provides an overview of the inputs and outputs of ACE.

ACE-FV3 (Watt-Meyer et al., 2023) is trained on output from FV3GFS (L. Zhou et al., 2019), the atmospheric model for the Global Forecast System (GFS) used for operational weather prediction. Training data was generated by running FV3GFS forced with an annually repeating climatology of rsdt, SIC, and SST, averaged from the period 1982-2012, keeping greenhouse gas and aerosol concentrations fixed. Each variable (see Fig. 1a) is available on a 6-hourly timescale on a grid with a 1° resolution and eight vertical levels. In total, 10 ensemble members, each with 10-year-long simulations, were used to train ACE-FV3.

ACE-EAM (Duncan et al., 2024) is trained on output from the E3SM Atmosphere Model (EAMv2), the atmospheric component of the Department of Energy’s Energy Exascale Earth System Model (E3SMv2 Golaz et al., 2022). Similar to ACE-FV3, ACE-EAM was trained on an annually repeating climatology of rsdt, SIC, and SST (averaged over 2005-2014, based on observations), while emissions were kept fixed at the level of 2010. A 42-year-long simulation was used to train ACE-EAM, with the same spatial and temporal resolution as ACE-FV3.

ACE2-ERA5 (Watt-Meyer et al., 2024) is the only version we use that is trained on historical data, based on output from the fifth generation ECMWF reanalysis (ERA5 Hers-

**a** Input-output diagram of ACE



**b** ACE Green's function simulations

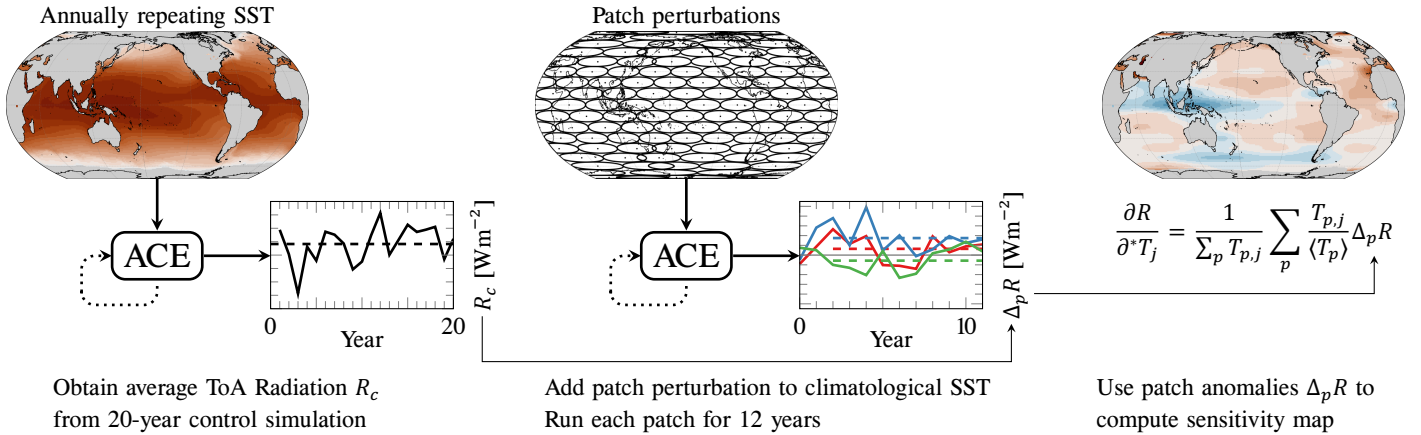


**Figure 1.** Overview of ACE and the Green's function simulations. **a** Schematic of the inputs and outputs of ACE (based on Watt-Meyer et al., 2023, see their Table 1 for more details). Here, we use SST forcing and ToA radiative fluxes as output. **b** Schematic of the Green's function simulations with ACE (based on Bloch-Johnson et al., 2024, see their Figure 1 for more details).

bach et al., 2020). ERA5 data is regridded to a  $1^\circ$  horizontal resolution and eight vertical levels. The training data consists of three periods: 1940-1995, 2011-2019, and 2021-2022, while other years are kept for validation and testing. Apart from rsdt, SIC, and SST, ACE2-ERA5 is also forced by  $\text{CO}_2$  concentration.

All versions of ACE have been previously trained on different datasets and underlying atmospheric models. If ACE is a good emulator, it will carry over the same strengths and shortcomings of the training data. GCMs are commonly tuned to obtain realistic global-mean ToA radiative fluxes, enforcing energetic constraints (Hourdin et al., 2017; Wild, 2020). For example, in the coupled GCM E3SM, the atmospheric component EAMv2 is tuned to obtain a near-zero ToA radiative flux in a long pre-industrial control simulation (Golaz et al., 2022). Therefore, we might expect ACE-EAM to carry over this energy constraint. In contrast, numerical weather prediction models like FV3GFS are not tuned to reproduce the global ToA radiation, as they are not necessarily built for predictions on climate timescales, which require energy constraints. Similarly, ERA5 is constrained by assimilating observations, but does not assimilate observations of the ToA radiative fluxes (Hersbach et al., 2020). Wild and Bosilovich (2024) showed that ERA5 performs reasonably well in capturing the long-term average and internal variability of the net ToA radiation, but does not reproduce the historical trend of the global-mean energy imbalance  $N$ . Although physical constraints can be imposed on ACE2, ACE2-ERA5 only conserves the global mean moisture budget, not the energy budget (Watt-Meyer et al., 2024).

## 2.2 Green’s function experiments

The Green’s function method is outlined in Fig. 1b. We generally follow the protocol as outlined by the Green’s Function Model Intercomparison Project (GFMIP, Bloch-Johnson et al., 2024), although we make some minor changes when applying it to ACE. The GFMIP protocol in Bloch-Johnson et al. (2024) is designed to investigate differences across GCMs by standardizing the simulations. We focus here on the Green’s function for the globally averaged net ToA radiation  $R$ , defined as the sum of incoming solar radiation, reflected solar radiation, and outgoing longwave radiation at the top of the atmosphere (ToA; positive downwards). However, we note that the same protocol can be applied to any atmospheric variable that is output by ACE, without performing additional model runs. In the following, we refer to the “Green’s function” as the partial derivative of  $R$  with respect to local SST, but note that the Green’s function method can be more generally applied to different simulated variables.

First, we run a 20-year control simulation for each version of ACE forced with an annually repeating climatology. For ACE-FV3 and ACE-EAM, we use the climatology it was trained on, while for ACE2-ERA5 we compute the ERA5 climatology from 1971-2020 (see last column of Supplemental Table S1). The climatology is calculated by averaging the values in all years 1971-2020 for every grid point and 6-hourly time step. Although ACE provides output every 6 hours, we only save monthly averages for each run. The 20-year-mean, globally averaged, ToA radiation of the control simulation,  $R_c$  (dashed black line in Fig. 1b), is used as the reference state for the Green’s function simulations.

Next, we perform patch simulations, each with the same initial conditions taken from the end of the control run. We use the same annually repeating climatology, but add a local perturbation to the sea surface temperature, given by

$$T_p(\varphi, \vartheta) = \begin{cases} A \cos^2\left(\pi \frac{\varphi - \varphi_p}{\delta\varphi_p}\right) \cos^2\left(\pi \frac{\vartheta - \vartheta_p}{\delta\vartheta_p}\right) & \begin{cases} \varphi - \varphi_p \in [-\delta\varphi_p, \delta\varphi_p] \\ \vartheta - \vartheta_p \in [-\delta\vartheta_p, \delta\vartheta_p] \end{cases} \\ 0 & \text{elsewhere} \end{cases}. \quad (1)$$

Here,  $A$  is the amplitude of the perturbation,  $(\varphi, \vartheta)$  are latitude and longitude,  $(\varphi_p, \vartheta_p)$  denotes the center of the perturbation, and  $(\delta\varphi_p, \delta\vartheta_p)$  are the latitudinal and longitudinal widths of the perturbation. We use the patch layout of Bloch-Johnson et al. (2024, see their

Table 1); a sketch of the different patches is shown in Fig. 1b, where for each patch the contour at  $A/2$  is shown. In total, there are 109 different patches that cover the entire globe. We perform simulations for positive ( $A = +2\text{K}$ ) and negative ( $A = -2\text{K}$ ) perturbations, with each patch run for 12 years, totalling to 2616 simulation years. The ToA radiation of each patch simulation is averaged over the last 10 years, allowing for two years of spin-up.

Finally, the difference  $\Delta_p R = R_p - R_c$  between the patch radiation  $R_p$  and the control  $R_c$  (colored dashed lines in Fig. 2b) is used to calculate the Green’s function. At each grid-box  $j = (\varphi_j, \vartheta_j)$ , the Green’s function of the ToA radiation  $R$  is given by

$$\frac{\partial R}{\partial^* T_j} = \frac{1}{\sum_p T_{p,j}} \sum_p \frac{T_{p,j}}{\langle T_p \rangle} \Delta_p R \quad (2)$$

Here,  $\langle T_p \rangle = \sum_j a_j T_{p,j}$ , the weighted average of the patch temperature, with  $a_j$  the ice-free ocean area of grid-box  $j$  normalized to the total ice-free ocean area. The asterisk in Eq. (2) denotes the area-normalized derivative, related to the gradient as  $\partial R / \partial T_j = a_j \partial R / \partial^* T_j$ . The normalized derivative makes the quantity independent of grid-box area and allows for a direct comparison between models with different spatial resolution (Bloch-Johnson et al., 2024). A separate Green’s function is calculated for positive and negative patch perturbations, and the average of the two is taken as the final Green’s function.

We compare the Green’s functions of ACE to Green’s functions of five GCMs that were calculated from the average of positive and negative patch simulations: CAM5 (Neale et al., 2010; C. Zhou et al., 2017), CanESM5 (Swart et al., 2019), ECHAM6 (Stevens et al., 2013; Alessi & Rugenstein, 2023), GFDL-AM4 (Zhao et al., 2018; Zhang et al., 2023), and HadAM3 (Pope et al., 2000). These all differ slightly in their patch setup and control climatology, but use a similar protocol as described above (see Figure 2 in Bloch-Johnson et al., 2024). Here, we qualitatively compare the Green’s functions of the traditional, physics-based GCMs to the ones obtained with different ACE versions. The GCM Green’s functions are all scaled to a common  $3.75^\circ \times 2.5^\circ$  grid (the lowest resolution among the GCMs) using a conservative method with periodic boundary conditions.

### 3 Results

#### 3.1 ACE Green’s function sensitivity maps

In Fig. 2, we compare the Green’s functions of ACE-FV3, ACE-EAM, and ACE2-ERA5 with the average Green’s function across the five GCMs. The sensitivity maps visualize how the global-mean ToA radiation  $R$  responds when increasing the surface temperature in a single grid-box. Thus, they represent the sum of local and remote radiative feedbacks to changing sea surface temperature. The reanalysis-based Green’s function of ACE2-ERA5 (Fig. 2a) is qualitatively similar to the GCM results (Fig. 2b), although the amplitude of the local feedbacks is lower. Similarly, ACE-EAM (Fig. 2c) finds the general structure of the GCM Green’s function. In contrast, ACE-FV3 (Fig. 2d) shows a much noisier map.

Fig. 2a depicts the first Green’s function that is entirely based on reanalysis data. As explained in section 2.1, ERA5 constrains its predictions by assimilating observations, but does not use direct observations of the ToA radiative imbalance (Hersbach et al., 2020). The fact that ACE2-ERA5 is able to reproduce the main features of the GCM Green’s function (Fig. 2a versus b) is not trivial, and indicates that ACE2-ERA5 captures the main physical mechanisms of the radiative feedbacks. Still, there are some regional differences between the ACE2-ERA5 and GCM Green’s functions and the amplitude of the local feedbacks is lower in ACE2-ERA5. We emphasize that the *true* sensitivity map is unknown, and thus there is no a priori reason to trust the GCMs over ACE2-ERA5.

The ACE2-ERA5 Green’s function qualitatively aligns with our physical understanding of local and remote feedbacks. Specifically, we expect to see negative feedbacks in regions of deep convection, such as the tropical West Pacific, and positive feedbacks in regions of

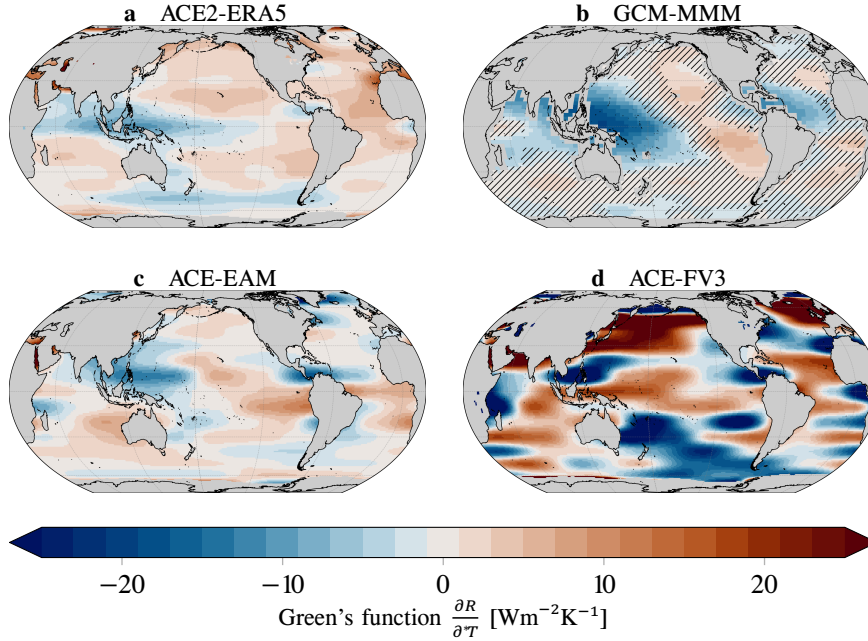


**Figure 2.** Green’s functions of (a) ACE2-ERA5, (b) Multi-model mean (MMM) of 5 GCMs (Bloch-Johnson et al., 2024), (c) ACE-EAM, and (d) ACE-FV3. Note that the resolution of ACE is  $1^\circ \times 1^\circ$ , while the GCMs are on a  $3.75^\circ \times 2.5^\circ$  grid. Hatching in **b** indicates regions where at least one GCM disagrees on the sign of the Green’s function.

subsidence, such as the subtropical East Pacific. This behavior is mostly driven by the sensitivity of shallow marine stratocumulus clouds to local and remote changes in surface temperature (C. Zhou et al., 2016; Andrews et al., 2018; Myers et al., 2021, 2023). For example, local warming in the region of the low cloud decks in the East Pacific, off the coast of South America, leads to a decrease in low-level clouds, which in turn decreases the outgoing shortwave radiation (positive feedback). In contrast, warming the surface in the West Pacific warm pool leads to warmer upper troposphere in the subtropical East Pacific due to teleconnections. This warming makes the air more stable in regions with low clouds, increasing the amount of clouds and therefore the outgoing shortwave radiation (negative feedback) (Rugenstein, Zelinka, et al., 2023).

GCMs capture the same physical mechanisms of feedbacks: they agree on the sign of the Green’s function in regions of deep convection and subsidence (Fig. 2b). The ACE-EAM Green’s function (Fig. 2c) has a similar structure, indicating that ACE-EAM has learned the relationship between SST and  $R$  from EAMv2. Still, since ACE-EAM was trained on an annually repeating climatology, there is no inherent reason why this relationship would be preserved when forcing it with patch perturbations. Even if a  $\pm 2$  K perturbation falls within the local seasonal cycle of SST, at some time of the year the perturbed SST will be outside the range of the training data. This is especially true for the tropics, where the seasonal cycle is small, and large regions never experience variations larger than  $\pm 2$  K (Supplemental Figure S1a). This means that the Green’s function simulations are truly out-of-distribution for ACE-EAM, pointing to the possibility of using ACE to investigate future climates.

In contrast, ACE-FV3 fails to capture the expected relationship between SST and  $R$  (Fig. 2d). This might be because numerical weather prediction models like FV3GFS (on which ACE-FV3 was trained) are not energetically closed. Moreover, similar to ACE-



EAM, the Green’s function simulations sample ACE-FV3 outside of its trained domain (Supplemental Figure S1b). Although the sign of the feedback could be interpreted as correct in some regions, such as the Philippines and Central America, other regions show responses opposite from what we expect, such as the subtropical East Pacific. The ACE-FV3 Green’s function shows a pattern similar to the patch layout (see Fig. 1b), indicating that responses can vary considerably between adjacent patch perturbations. ACE-FV3 tends to overestimate the variability of  $R$  on yearly timescales (Supplemental Figure S2), such that longer temporal averages might be necessary to filter out the noise. However, lengthening the patch simulations to 30 years did not improve the results.

### 3.2 Historical ToA radiative response to surface warming

The Green’s functions not only give us physical insight into local feedbacks, but they can be used to estimate the radiative response to any sea surface temperature forcing. The Green’s functions depict the partial derivative of  $R$  with respect to local SST ( $T_j$ ), such that in a linear approximation

$$R = \sum_j a_j \frac{\partial R}{\partial T_j} T_j + \mathcal{O}(T^2). \quad (3)$$

That is, given any SST map, the ToA radiation can be approximated by using equation (3). To test whether or not the ACE Green’s functions can be used for this purpose, we convolve the Green’s function with SST maps from the AMIP dataset (Taylor et al., 2000), which contains observed SST from 1870-2020. The resulting time series of  $R$  is shown in Fig. 3. Each line was calculated by conservatively regridding the AMIP SST to ACE’s native grid, multiplying it with the Green’s function, and averaging the result weighted by the ice-free ocean area. As a reference, we show the predictions from the GCM Green’s functions as gray lines calculated in the same way as the ACE Green’s function predictions.

Although we do not know the absolute truth for the historical  $R$ , we expect it to become more negative in a warming world. That is, with increasing global-mean temperature, we expect a greater outgoing energy flux to counteract the forcing. This decline is not predicted by the ACE2-ERA5 Green’s function (Fig. 3, red line). Moreover, the variability of  $R$  is much smaller than in the observed ToA radiative imbalance (see Supplemental Figure S3). Similarly, the ACE-EAM Green’s function does not predict a realistic  $R$ , although it predicts a slight decrease in the last two decades. The annual variability in the predicted  $R$  from ACE-FV3 is larger, but shows unrealistic decadal variations.

Even though the ACE2-ERA5 sensitivity map looks similar to the GCM Green’s functions (Fig. 2), its predicted ToA radiative response  $R$  does not (Fig. 3). This could be due to ACE2-ERA5 not capturing the full response of  $R$  to SST, the Green’s function protocol, or both. To test the former, we run ACE2-ERA5 forced with historical SST from ERA5, and compare the predicted ToA radiation with the “truth” from ERA5 (Supplemental Figure S3). The output of this historical run reflects how well ACE2-ERA5 performs in simulating the ToA radiative imbalance as compared to the underlying dataset (ERA5 reanalysis). The ERA5 data itself does not capture the correct trend in the ToA radiation, but performs well on its variability, as compared to direct observations (CERES-EBAF, Loeb et al., 2018). Moreover, even over the training period (1940-1995), ACE2-ERA5 is not able to reproduce the correct ToA radiation on yearly timescales, indicating that ACE2-ERA5 misses some of the response of  $R$  to SST.

To further test the Green’s function setup, we also calculate the ACE2-ERA5 Green’s function for  $A = \pm 4$  K (Supplemental Figure S4). Green’s functions for  $A = \pm 2$  K and  $A = \pm 4$  K are qualitatively similar, indicating that the ACE2-ERA5 Green’s function is somewhat robust to the amplitude of the patches. However, the predicted  $R$  is very sensitive to the patch amplitude and its sign. In ACE2-ERA5, using the Green’s function with

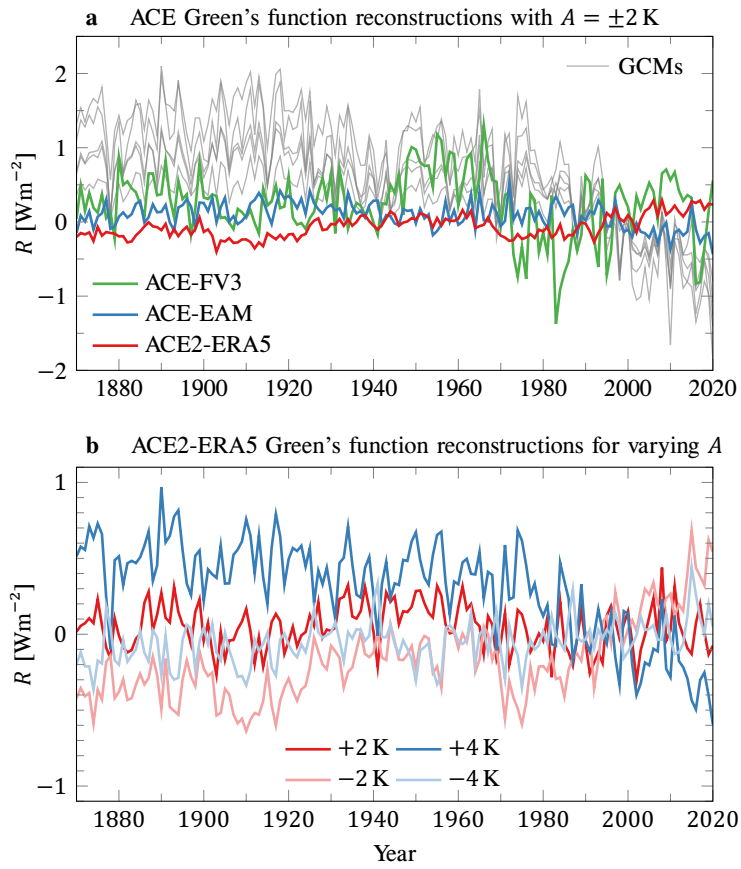


**Figure 3.** Historical reconstruction of the net ToA radiation  $R$ , formed by convolving the Green's functions with AMIP sea surface temperature anomalies with respect to 1971-2020.

$A = +4\text{K}$  (positive patch perturbations only), the reconstructed  $R$  looks more realistic (dark blue line in Fig. 3b) than the  $A = \pm 2\text{K}$  reconstruction (red in line Fig. 3a).

In general, Green’s function predictions are highly nonlinear in the sign of  $A$  (Bloch-Johnson et al., 2024). Using  $A > 0$  only, the Green’s functions mostly predict a decrease in  $R$  over the historical period, while using  $A < 0$  only, the Green’s function mostly predict an increase in  $R$  (Supplemental Figure S5). This is true for all versions of ACE (apart from ACE2-ERA5 with  $A = +2\text{K}$ ), but also for the GCMs (Supplemental Figure S5b). Surprisingly, the reconstructed  $R$  from ACE-FV3 is comparable to  $R$  based on the GCM Green’s functions, even though its Green’s function did not follow our expectations (Fig. 2d). This might be due to competing biases in the ACE-FV3 Green’s function, which cancel out in the reconstruction. These results point to some of the limitations of the Green’s function method, discussed in more detail in the following section.

## 4 Discussion

Estimating the ToA radiative response to surface warming is a topic of debate, and the true relationship between  $R$  and SST is unknown (e.g., Sherwood et al., 2020; Rugenstein, Zelinka, et al., 2023). To study this problem, we have thus far had to rely on GCMs because the observational record is too short to find a robust relationship between the two (Thompson et al., in review; Fredericks, Rugenstein, & Thompson, in prep.). Even if a longer record existed, we can only directly observe the top-of-atmosphere radiative imbalance  $N = F + R$  and not  $R$  itself. Because we cannot turn off or measure the forcing  $F$  in the real world, we only have access to the internal variability of the ToA fluxes (which are assumed to be similar for  $N$  and  $R$ , e.g., Dessler & Forster, 2018). Thus, when using observations to constrain future projections, we need to assume that internal variability of  $R$  also explains its forced response (Rugenstein et al., 2025).

Green’s function experiments with ACE2-ERA5 allow us to overcome these issues. Because the Green’s functions are calculated by only changing the SST, all other forcing agents (e.g.,  $\text{CO}_2$  or aerosols) are essentially kept fixed, such that  $F = 0$  and  $N = R$ . This is similar to performing AMIP experiments in GCMs (Webb et al., 2017). However, these experiments are costly to run, have their own model-specific biases and unknowns in the physics, and require coordinated protocol efforts, for which the development cycle usually lags behind observations. Thus, if we are able to trust the ACE2-ERA5 Green’s function, this method offers a new way to remove the radiative forcing from the *observed* climate system. That is, the ACE2-ERA5 Green’s function represents the historical, reanalysis-based, climate with  $F = 0$ .

As we have shown, however, ACE2-ERA5 may not yet be ready for this purpose. Since ERA5 is a reanalysis product, it comes with its own biases with respect to observations (e.g., Wild & Bosilovich, 2024; Dussin, 2025). These biases are propagated to ACE2-ERA5, even if the emulator would exactly replicate the behavior of ERA5. Overall, machine-learning methods are known to perform poorly on out-of-distribution tasks. Because ACE2-ERA5 is trained on historical reanalysis data, it is not expected to perform well in far out-of-distribution scenarios, such as quadrupling of  $\text{CO}_2$  concentration or a much warmer world (Watt-Meyer et al., 2024). Given this, the fact that ACE2-ERA5 is able to reproduce the GCM Green’s function qualitatively is a big achievement, and promising for further development of climate emulators. Even for patch perturbations of larger amplitude ( $A = \pm 4\text{K}$ ), the ACE2-ERA5 Green’s functions remain realistic (Supplemental Figure S4). ACE2 allows for the inclusion of physical constraints, which was used to conserve the global mean moisture budget in ACE2-ERA5 (Watt-Meyer et al., 2024). Using this feature to constrain the global energy budget would be a possible way forward to better represent the ToA radiative response to surface warming. We hypothesize that a closed energy budget is a necessary condition for climate emulators to accurately make predictions.

Besides the Green’s function method, other approaches have been used to study the spatial relationship between  $R$  and SST (e.g., Bloch-Johnson et al., 2020; Falasca et al., 2025; Rugenstein et al., 2025; Thompson et al., in review; Van Loon et al., 2025b; Fredericks, Rugenstein, & Thompson, in prep.). These different methods generally agree on the overall structure of the sensitivity maps (e.g., Fig. 2a-c), suggesting that this is a robust feature across models. However, approaches can differ in the specifics of the sensitivity maps, such as the importance of small-scale features or the amplitude of the local feedbacks, while still being able to reproduce  $R$  with similar skill (Rugenstein et al., 2025; Fredericks, Van Loon, et al., in prep.). Because ACE2-ERA5 is computationally very efficient, it might be possible to use it to investigate some of these differences, for example, by running different patch setups and amplitudes or multiple patches at once to investigate nonlinearities.

By performing Green’s function simulations, the sensitivity of climate emulators can be tested. Ullrich et al. (2025) called for systematic testing of machine learning-based Earth system models in order to demonstrate their use for scientific discovery in the same manner as physics-based GCMs. The Green’s function method could be one of these tests, as it probes how well the emulator performs in an idealized setting well outside of its trained domain. The Green’s function sensitivity maps offer initial insight into whether or not the emulator responds realistically to variations in SST, and can be directly compared to GCMs. By looking at the response to individual patch perturbations, it is possible to investigate causal relationships between SST and other variables.

However, Green’s function simulations come with its own limitations. Even across different GCMs, there are large variations in the representation of the sensitivities, and the absolute truth is not known (Bloch-Johnson et al., 2024). Although we have some theories about the physical processes that govern positive or negative feedbacks in the sensitivity maps (e.g., low cloud feedbacks in marine stratocumulus regions), we do not know the exact extent, spatial detail, or amplitude of the local feedbacks (Myers et al., 2021, 2023; Ceppi et al., 2024). Aside from the model used, the Green’s functions depend on choices of the exact patch setup or length of the simulations and do not take into account nonlinearities of the climate system (Bloch-Johnson et al., 2021; Williams et al., 2023). For example, the reconstructed  $R$  depends on the amplitude of the patch perturbation (Fig. 3b and Supplemental Figure S5). This makes comparing sensitivity maps between emulators more of a qualitative test than a quantitative assessment.

In summary, we have performed Green’s function simulation with different versions of the Ai2 Climate Emulator (ACE). The Green’s function of ACE2-ERA5, which was trained on reanalysis data, shows promising qualitative agreement with expectations, but cannot recreate a realistic top-of-atmosphere radiative response to surface warming in the historical period. We conclude that Green’s function experiments offer a way to test climate emulators in an idealized setting and investigate their sensitivity to external forcing. Such simulations could be part of a broader testbed for machine learning-based atmospheric models to assess their viability for scientific discovery.

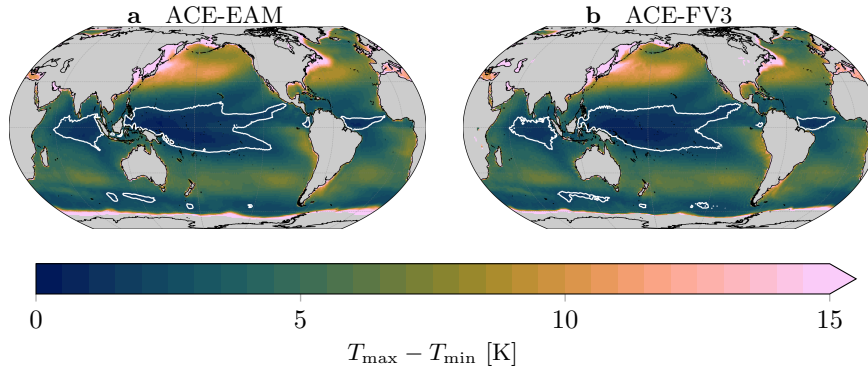
## Open Research Section

All ACE code, checkpoints, and forcing data are freely available through the Ai2 Hugging Face repository at <https://huggingface.co/collections/allenai/ace-67327d822f0f0d8e0e5e6ca4>. The code used to perform the Green’s function simulations is available at <https://github.com/SnnVL/GF4ACE> and output data is available at <https://doi.org/10.5061/dryad.d2547d8cf> (Van Loon et al., 2025a). The Green’s functions from CAM5, CanESM5, ECHAM6, GFDL-AM4, and HadAM3 were obtained from Bloch-Johnson et al. (2023). Monthly historical temperature (AMIP) was downloaded from <https://gfmip.org>.

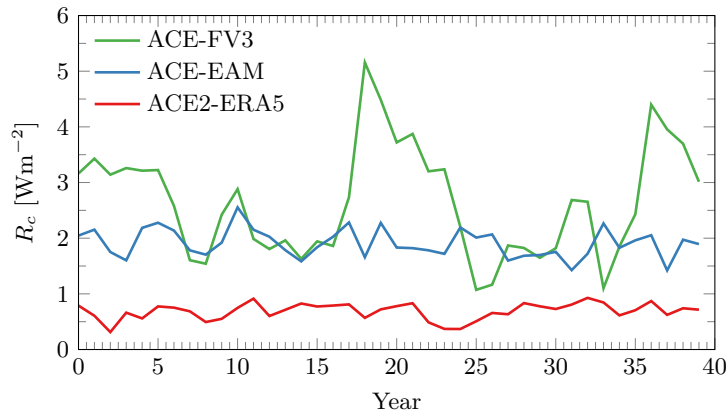
**Acknowledgments**

This work was supported, in part, by the Regional and Global Model Analysis program area of the U.S. Department of Energy's (DOE) Office of Biological and Environmental Research (BER) as part of the Program for Climate Model Diagnosis and Intercomparison project. EAB was also supported by a grant from the Heising-Simons Foundation.

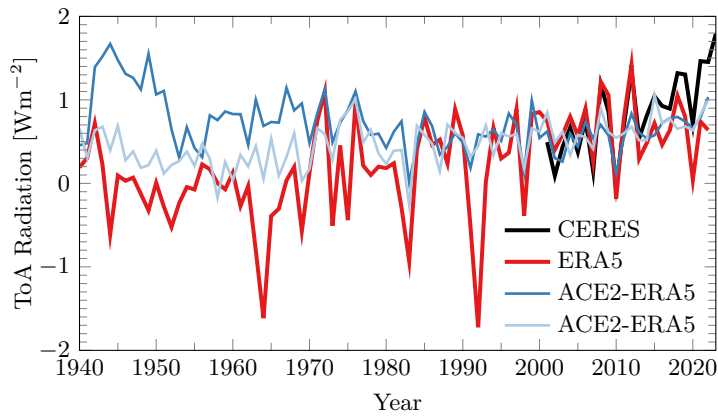
## Supporting Information



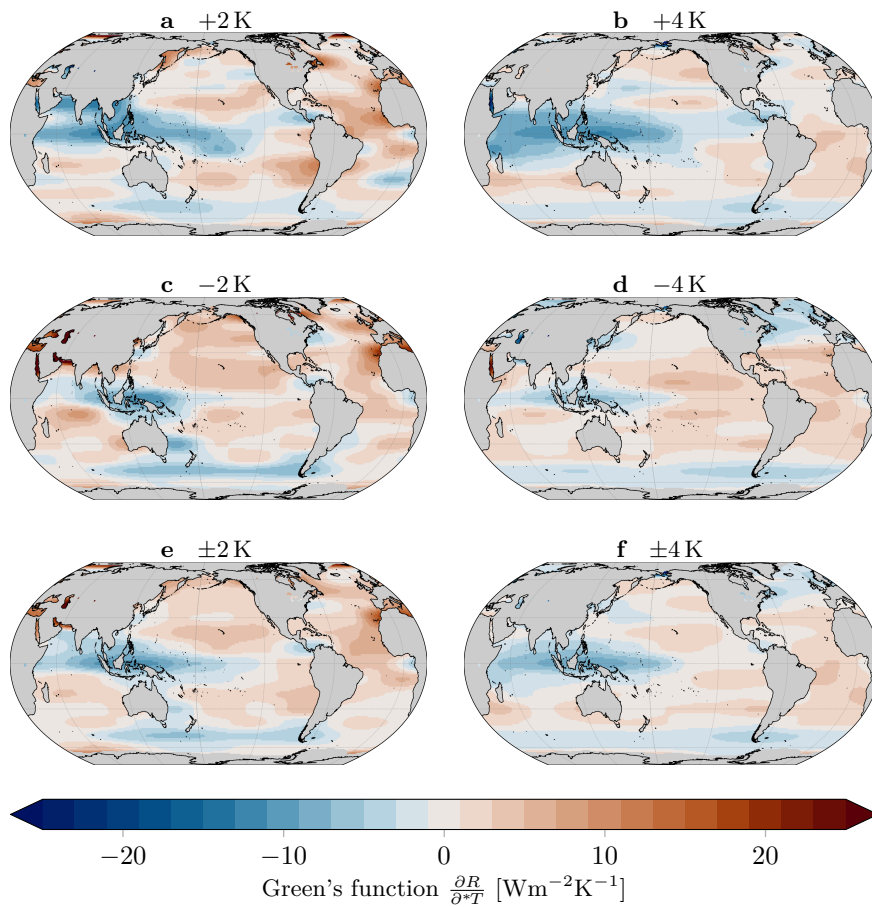
**Supporting Information Fig. S1.** Amplitude of the seasonal cycle of the climatology used to train ACE-EAM (a) and ACE-FV3 (b). The amplitude is calculated by taking the difference between the maximum and minimum of the six-hourly data in the annual climatology. The white contour demarcates the region where the amplitude is smaller than 2 K, the amplitude of the patch perturbations used in the Green's function simulations.



**Supporting Information Fig. S2.** Top-of-atmosphere (ToA) radiation of the control run for three different versions of ACE, forced by an annually repeating climatology (see Table S1). Only the first twenty years are used to construct the Green's function.

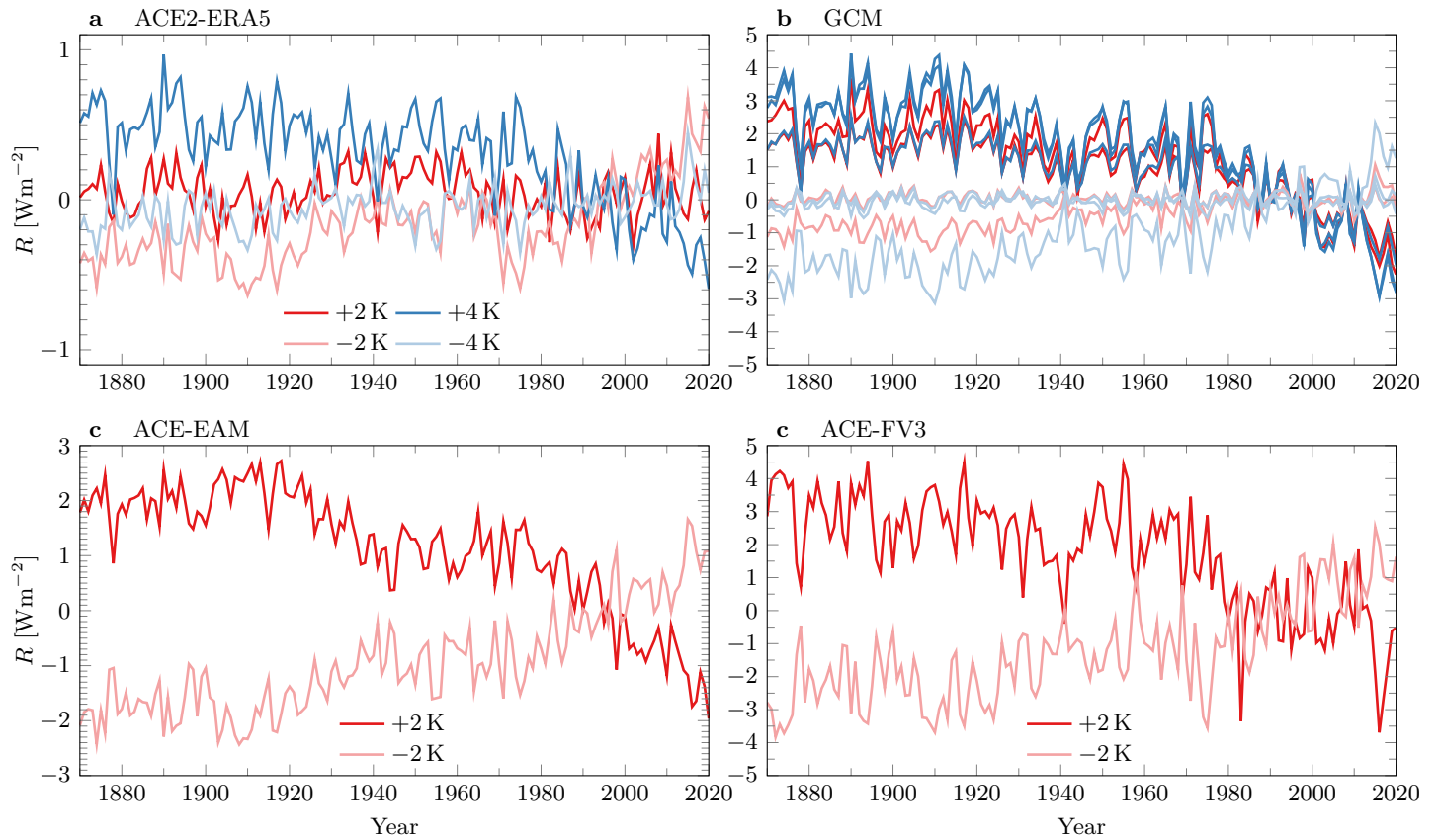


**Supporting Information Fig. S3.** Top-of-atmosphere (ToA) radiation in ERA5 (red line) compared to two historical runs in ACE2-ERA5 (blue lines), starting from different initial conditions but using the same forcing. The black lines shows the observed ToA radiation from CERES-EBAF (Loeb et al., 2018). The blue lines are calculated by forcing the ACE2-ERA5 model with ERA5 data from 1940-2022 for the incoming solar radiation, sea ice concentration, sea surface temperature, and CO<sub>2</sub> concentration. Because historical data is used, here the ToA radiation contains a forced signal, and is thus showing the ToA radiative imbalance  $N = F + R$ , with  $F$  the radiative forcing.



**Supporting Information Fig. S4.** Green's functions of ACE2-ERA5 for different patch amplitudes  $A$ . The top row (a-b) shows positive patches, the middle row (c-d) negative patches, and the bottom row (e-f) the average of the positive and negative patch Green's functions.





**Supporting Information Fig. S5.** Historical reconstruction of the net ToA radiation  $R$ , formed by convolving the Green's functions computed from different patch amplitudes  $A$  with AMIP sea surface temperature anomalies with respect to 1971-2020. Panels **a**, **c**, and **d** show the reconstructions from different versions of ACE (ACE2-ERA5, ACE-EAM, and ACE-FV3, respectively). In panel **b**, reconstructions from the GCM Green's functions are shown (Bloch-Johnson et al., 2023). Every line represents a different GCM; the blue lines show GCMs that used  $A = \pm 4\text{K}$ , while the red lines show the GCMs that used  $A = \pm 2\text{K}$ .

**Supporting Information Table S1.** Overview of different ACE checkpoints and Green’s function forcing data.

Name	Training model	Training data	control climatology
ACE-FV3 <sup>a</sup>	FV3GFS <sup>b</sup>	1982-2012 climatology	1982-2012
ACE-EAM <sup>c</sup>	EAMv2 <sup>d</sup>	2005-2014 climatology	2005-2014
ACE2-ERA5 <sup>e</sup>	ERA5 <sup>f</sup>	1940-1995, 2011-2019, 2021-2022	1971-2020

<sup>a</sup> Watt-Meyer et al. (2023). <sup>b</sup> L. Zhou et al. (2019). <sup>c</sup> Duncan et al. (2024). <sup>d</sup> Golaz et al. (2022). <sup>e</sup> Watt-Meyer et al. (2024). <sup>f</sup> Hersbach et al. (2020).

## References

- Alessi, M. J., & Rugenstein, M. A. A. (2023). Surface Temperature Pattern Scenarios Suggest Higher Warming Rates Than Current Projections. *Geophysical Research Letters*, *50*(23), e2023GL105795. doi: 10.1029/2023GL105795
- Andrews, T., Bodas-Salcedo, A., Gregory, J. M., Dong, Y., Armour, K. C., Paynter, D., ... Liu, C. (2022). On the Effect of Historical SST Patterns on Radiative Feedback. *Journal of Geophysical Research: Atmospheres*, *127*(18), e2022JD036675. doi: 10.1029/2022JD036675
- Andrews, T., Gregory, J. M., Paynter, D., Silvers, L. G., Zhou, C., Mauritsen, T., ... Titchner, H. (2018). Accounting for Changing Temperature Patterns Increases Historical Estimates of Climate Sensitivity. *Geophysical Research Letters*, *45*(16), 8490-8499. doi: 10.1029/2018GL078887
- Andrews, T., Gregory, J. M., & Webb, M. J. (2015). The Dependence of Radiative Forcing and Feedback on Evolving Patterns of Surface Temperature Change in Climate Models. *Journal of Climate*, *28*(4), 1630-1648. doi: 10.1175/JCLI-D-14-00545.1
- Barsugli, J. J., & Sardeshmukh, P. D. (2002). Global Atmospheric Sensitivity to Tropical SST Anomalies throughout the Indo-Pacific Basin. *Journal of Climate*, *15*(23), 3427 - 3442. doi: 10.1175/1520-0442(2002)015<3427:GASTTS>2.0.CO;2
- Bloch-Johnson, J., Rugenstein, M., & Abbot, D. S. (2020). Spatial Radiative Feedbacks from Internal Variability Using Multiple Regression. *Journal of Climate*, *33*(10), 4121 - 4140. doi: 10.1175/JCLI-D-19-0396.1
- Bloch-Johnson, J., Rugenstein, M., Alessi, M., Proistosescu, C., Zhao, M., Zhang, B., ... Zhou, C. (2023). Data for "The Green’s Function Model Intercomparison Project (GFMIIP) Protocol". Zenodo. doi: 10.5281/zenodo.10414728
- Bloch-Johnson, J., Rugenstein, M., Stolpe, M. B., Rohrschneider, T., Zheng, Y., & Gregory, J. M. (2021). Climate Sensitivity Increases Under Higher CO2 Levels Due to Feedback Temperature Dependence. *Geophysical Research Letters*, *48*(4), e2020GL089074. (e2020GL089074 2020GL089074) doi: 10.1029/2020GL089074
- Bloch-Johnson, J., Rugenstein, M. A. A., Alessi, M. J., Proistosescu, C., Zhao, M., Zhang, B., ... Zhou, C. (2024). The Green’s Function Model Intercomparison Project (GFMIIP) Protocol. *Journal of Advances in Modeling Earth Systems*, *16*(2), e2023MS003700. (e2023MS003700 2023MS003700) doi: https://doi.org/10.1029/2023MS003700
- Bonev, B., Kurth, T., Hundt, C., Pathak, J., Baust, M., Kashinath, K., & Anandkumar, A. (2023). *Spherical Fourier Neural Operators: Learning Stable Dynamics on the Sphere*. Retrieved from <https://arxiv.org/abs/2306.03838>
- Bracco, A., Brajard, J., Dijkstra, H. A., Hassanzadeh, P., Lessig, C., & Monteleoni, C. (2025). Machine learning for the physics of climate. *Nature Reviews Physics*, *7*(1), 6-20. doi: 10.1038/s42254-024-00776-3
- Branstator, G. (1985). Analysis of General Circulation Model Sea-Surface Temperature Anomaly Simulations Using a Linear Model. Part I: Forced Solutions. *Journal of*

- Atmospheric Sciences*, 42(21), 2225 - 2241. doi: 10.1175/1520-0469(1985)042<2225:AOGCMS>2.0.CO;2
- Cachay, S. R., Henn, B., Watt-Meyer, O., Bretherton, C. S., & Yu, R. (2024). *Probabilistic Emulation of a Global Climate Model with Spherical Diffusion*. Retrieved from <https://arxiv.org/abs/2406.14798>
- Ceppi, P., Myers, T. A., Nowack, P., Wall, C. J., & Zelinka, M. D. (2024). Implications of a Pervasive Climate Model Bias for Low-Cloud Feedback. *Geophysical Research Letters*, 51(20), e2024GL110525. doi: 10.1029/2024GL110525
- Cresswell-Clay, N., Liu, B., Durran, D., Liu, A., Espinosa, Z. I., Moreno, R., & Karlbauer, M. (2024). *A Deep Learning Earth System Model for Stable and Efficient Simulation of the Current Climate*. Retrieved from <https://arxiv.org/abs/2409.16247>
- Dessler, A. E., & Forster, P. M. (2018). An Estimate of Equilibrium Climate Sensitivity From Interannual Variability. *Journal of Geophysical Research: Atmospheres*, 123(16), 8634-8645. doi: 10.1029/2018JD028481
- Dong, Y., Proistosescu, C., Armour, K. C., & Battisti, D. S. (2019). Attributing Historical and Future Evolution of Radiative Feedbacks to Regional Warming Patterns using a Green's Function Approach: The Preeminence of the Western Pacific. *Journal of Climate*, 32(17), 5471 - 5491. doi: 10.1175/JCLI-D-18-0843.1
- Duncan, J. P. C., Wu, E., Golaz, J.-C., Caldwell, P. M., Watt-Meyer, O., Clark, S. K., ... Bretherton, C. S. (2024). Application of the AI2 Climate Emulator to E3SMv2's Global Atmosphere Model, With a Focus on Precipitation Fidelity. *Journal of Geophysical Research: Machine Learning and Computation*, 1(3), e2024JH000136. doi: <https://doi.org/10.1029/2024JH000136>
- Dussin, R. (2025). Four Generations of ECMWF Reanalyses: An Overview of the Successes in Modeling Precipitation and Remaining Challenges for Freshwater Budget of Ocean Models. *Earth and Space Science*, 12(1), e2024EA003844. doi: 10.1029/2024EA003844
- Eyring, V., Collins, W. D., Gentile, P., Barnes, E. A., Barreiro, M., Beucler, T., ... Zanna, L. (2024). Pushing the frontiers in climate modelling and analysis with machine learning. *Nature Climate Change*, 14(9), 916-928. doi: 10.1038/s41558-024-02095-y
- Falasca, F., Basinski-Ferris, A., Zanna, L., & Zhao, M. (2025). *Diagnosing the pattern effect in the atmosphere-ocean coupled system through linear response theory*. Retrieved from <https://arxiv.org/abs/2408.12585>
- Flato, G., Marotzke, J., Abiodun, B., Braconnot, P., Chou, S., Collins, W., ... Rummukainen, M. (2013). Evaluation of climate models [Book Section]. In T. Stocker et al. (Eds.), *Climate change 2013: The physical science basis. contribution of working group I to the fifth assessment report of the intergovernmental panel on climate change* (p. 741-866). Cambridge, United Kingdom and New York, NY, USA: Cambridge University Press. Retrieved from <http://www.climatechange2013.org> doi: 10.1017/CBO9781107415324.020
- Forster, P., Storelvmo, T., Armour, K., Collins, W., Dufresne, J.-L., Frame, D., ... Zhang, H. (2021). The Earth's Energy Budget, Climate Feedbacks, and Climate Sensitivity [Book Section]. In V. Masson-Delmotte et al. (Eds.), *Climate Change 2021: The Physical Science Basis. Contribution of Working Group I to the Sixth Assessment Report of the Intergovernmental Panel on Climate Change* (p. 923-1054). Cambridge, UK and New York, NY, USA: Cambridge University Press. doi: 10.1017/9781009157896.009
- Fredericks, L., Rugenstein, M., & Thompson, D. W. J. (in prep.). An Observational Estimate of the Spatial Sensitivity Governing the Pattern Effect Using Regularized Linear Regression. *Journal of Climate*.
- Fredericks, L., Van Loon, S., Rugenstein, M., Thompson, D. W. J., Falasca, F., Basinski-Ferris, A., ... Bloch-Johnson, J. (in prep.). *Emerging methods for the development of radiative sensitivity maps from internal variability*.
- Golaz, J.-C., Van Roekel, L. P., Zheng, X., Roberts, A. F., Wolfe, J. D., Lin, W., ... Bader, D. C. (2022). The DOE E3SM Model Version 2: Overview of the Physical Model and Initial Model Evaluation. *Journal of Advances in Modeling Earth Systems*, 14(12),

- e2022MS003156. doi: 10.1029/2022MS003156
- Guan, H., Arcomano, T., Chattopadhyay, A., & Maulik, R. (2024). *LUCIE: A Lightweight Uncoupled Climate Emulator with long-term stability and physical consistency for O(1000)-member ensembles*. Retrieved from <https://arxiv.org/abs/2405.16297>
- Hersbach, H., Bell, B., Berrisford, P., Hirahara, S., Horányi, A., Muñoz-Sabater, J., ... Thépaut, J.-N. (2020). The ERA5 global reanalysis. *Quarterly Journal of the Royal Meteorological Society*, 146(730), 1999–2049. doi: 10.1002/qj.3803
- Hourdin, F., Mauritsen, T., Gettelman, A., Golaz, J.-C., Balaji, V., Duan, Q., ... Williamson, D. (2017). The Art and Science of Climate Model Tuning. *Bulletin of the American Meteorological Society*, 98(3), 589 - 602. doi: 10.1175/BAMS-D-15-00135.1
- IPCC. (2021). *Climate change 2021: The physical science basis. contribution of working group I to the sixth assessment report of the intergovernmental panel on climate change* (V. Masson-Delmotte et al., Eds.) [Book]. Cambridge, UK and New York, NY, USA: Cambridge University Press. Retrieved from [https://report.ipcc.ch/ar6/wg1/IPCC\\_AR6\\_WGI\\_FullReport.pdf](https://report.ipcc.ch/ar6/wg1/IPCC_AR6_WGI_FullReport.pdf) doi: 10.1017/9781009157896
- Kochkov, D., Yuval, J., Langmore, I., Norgaard, P., Smith, J., Mooers, G., ... Hoyer, S. (2024). Neural general circulation models for weather and climate. *Nature*, 632(8027), 1060-1066. doi: 10.1038/s41586-024-07744-y
- Loeb, N. G., Doelling, D. R., Wang, H., Su, W., Nguyen, C., Corbett, J. G., ... Kato, S. (2018). Clouds and the Earth’s Radiant Energy System (CERES) Energy Balanced and Filled (EBAF) Top-of-Atmosphere (TOA) Edition-4.0 Data Product. *Journal of Climate*, 31(2), 895 - 918. doi: 10.1175/JCLI-D-17-0208.1
- Myers, T. A., Scott, R. C., Zelinka, M. D., Klein, S. A., Norris, J. R., & Caldwell, P. M. (2021). Observational constraints on low cloud feedback reduce uncertainty of climate sensitivity. *Nature Climate Change*, 11(6), 501–507. doi: 10.1038/s41558-021-01039-0
- Myers, T. A., Zelinka, M. D., & Klein, S. A. (2023). Observational Constraints on the Cloud Feedback Pattern Effect. *Journal of Climate*, 36(18), 6533 - 6545. doi: 10.1175/JCLI-D-22-0862.1
- Neale, R. B., Chen, C.-C., Gettelman, A., Lauritzen, P. H., Park, S., Williamson, D. L., ... others (2010). Description of the NCAR community atmosphere model (CAM 5.0). *NCAR Tech. Note Ncar/tn-486+ STR*, 1(1), 1–12. doi: 10.5065/wgtk-4g06
- Pope, V. D., Gallani, M. L., Rowntree, P. R., & Stratton, R. A. (2000). The impact of new physical parametrizations in the Hadley Centre climate model: HadAM3. *Climate Dynamics*, 16(2), 123-146. doi: 10.1007/s003820050009
- Randall, D. A., Bitz, C. M., Danabasoglu, G., Denning, A. S., Gent, P. R., Gettelman, A., ... Thuburn, J. (2018). 100 Years of Earth System Model Development. *Meteorological Monographs*, 59, 12.1 - 12.66. doi: 10.1175/AMSMONOGRAPHS-D-18-0018.1
- Rugenstein, M., Dhame, S., Olonscheck, D., Wills, R. C. J., Watanabe, M., & Seager, R. (2023). Connecting the SST Pattern Problem and the Hot Model Problem. *Geophysical Research Letters*, 50(22), e2023GL105488. doi: 10.1029/2023GL105488
- Rugenstein, M., Van Loon, S., & Barnes, E. A. (2025). Convolutional neural networks trained on internal variability predict forced response of TOA radiation by learning the pattern effect. *Geophysical Research Letters*, 52, e2024GL109581. doi: 10.1029/2024GL109581
- Rugenstein, M., Zelinka, M., Karauskas, K. B., Ceppi, P., & Andrews, T. (2023). Patterns of Surface Warming Matter for Climate Sensitivity. *Eos*, 104. doi: 10.1029/2023EO230411.
- Seager, R., Cane, M., Henderson, N., Lee, D.-E., Abernathey, R., & Zhang, H. (2019). Strengthening tropical Pacific zonal sea surface temperature gradient consistent with rising greenhouse gases. *Nature Climate Change*, 9(7), 517–522. doi: 10.1038/s41558-019-0505-x
- Senior, C. A., & Mitchell, J. F. B. (2000). The time-dependence of climate sensitivity. *Geophysical Research Letters*, 27(17), 2685–2688. Retrieved from <http://dx.doi.org/10.1029/2000GL011373> doi: 10.1029/2000GL011373

- Sherwood, S. C., Webb, M. J., Annan, J. D., Armour, K. C., Forster, P. M., Hargreaves, J. C., ... Zelinka, M. D. (2020). An Assessment of Earth’s Climate Sensitivity Using Multiple Lines of Evidence. *Reviews of Geophysics*, 58(4). doi: 10.1029/2019RG000678
- Soden, B. J., Collins, W. D., & Feldman, D. R. (2018). Reducing uncertainties in climate models. *Science*, 361(6400), 326–327. doi: 10.1126/science.aau1864
- Stevens, B., Giorgetta, M., Esch, M., Mauritsen, T., Crueger, T., Rast, S., ... Roeckner, E. (2013). Atmospheric component of the MPI-M Earth System Model: ECHAM6. *Journal of Advances in Modeling Earth Systems*, 5(2), 146–172. doi: 10.1002/jame.20015
- Swart, N. C., Cole, J. N. S., Kharin, V. V., Lazare, M., Scinocca, J. F., Gillett, N. P., ... Winter, B. (2019). The Canadian Earth System Model version 5 (CanESM5.0.3). *Geoscientific Model Development*, 12(11), 4823–4873. doi: 10.5194/gmd-12-4823-2019
- Taylor, K. E., Williamson, D., & Zwiers, F. (2000). The sea surface temperature and sea-ice concentration boundary conditions for AMIP II simulations. *PCMDI Report No. 60*, 1–25.
- Thompson, D. W. J., Rugenstein, M., Forster, P., & Fredericks, L. (in review). An Observational Estimate of the Pattern Effect on Climate Sensitivity: The Importance of the Eastern Tropical Pacific and Land Areas. *Journal of Climate*.
- Ullrich, P. A., Barnes, E. A., Collins, W. D., Dagon, K., Duan, S., Elms, J., ... Rebassoo, F. O. (2025). *Recommendations for Comprehensive and Independent Evaluation of Machine Learning-Based Earth System Models*. Retrieved from <https://arxiv.org/abs/2410.19882>
- Van Loon, S., Rugenstein, M., & Barnes, E. A. (2025a). *GF4ACE – Data & Software for “[PAPER TITLE]”*. Dryad. doi: 10.5061/dryad.d2547d8cf
- Van Loon, S., Rugenstein, M., & Barnes, E. A. (2025b). *Observation-based estimate of Earth’s effective radiative forcing*. EarthArXiv. Retrieved from <https://doi.org/10.31223/X5FM8P>
- Watt-Meyer, O., Dresdner, G., McGibbon, J., Clark, S. K., Henn, B., Duncan, J., ... Bretherton, C. S. (2023). *ACE: A fast, skillful learned global atmospheric model for climate prediction*. Retrieved from <https://arxiv.org/abs/2310.02074>
- Watt-Meyer, O., Henn, B., McGibbon, J., Clark, S. K., Kwa, A., Perkins, W. A., ... Bretherton, C. S. (2024). *ACE2: Accurately learning subseasonal to decadal atmospheric variability and forced responses*. Retrieved from <https://arxiv.org/abs/2411.11268>
- Webb, M. J., Andrews, T., Bodas-Salcedo, A., Bony, S., Bretherton, C. S., Chadwick, R., ... Watanabe, M. (2017). The Cloud Feedback Model Intercomparison Project (CFMIP) contribution to CMIP6. *Geoscientific Model Development*, 10(1), 359–384. doi: 10.5194/gmd-10-359-2017
- Wild, M. (2020). The global energy balance as represented in CMIP6 climate models. *Climate Dynamics*, 55(3), 553–577. doi: 10.1007/s00382-020-05282-7
- Wild, M., & Bosilovich, M. G. (2024). The Global Energy Balance as Represented in Atmospheric Reanalyses. *Surveys in Geophysics*, 45(6), 1799–1825. doi: 10.1007/s10712-024-09861-9
- Williams, A. I. L., Jeevanjee, N., & Bloch-Johnson, J. (2023). Circus Tents, Convective Thresholds, and the Non-Linear Climate Response to Tropical SSTs. *Geophysical Research Letters*, 50(6), e2022GL101499. doi: 10.1029/2022GL101499
- Wills, R. C. J., Dong, Y., Proistosescu, C., Armour, K. C., & Battisti, D. S. (2022). Systematic Climate Model Biases in the Large-Scale Patterns of Recent Sea-Surface Temperature and Sea-Level Pressure Change. *Geophysical Research Letters*, 49(17), e2022GL100011. doi: 10.1029/2022GL100011
- Xiang, B., Zhao, M., Held, I. M., & Golaz, J.-C. (2017). Predicting the severity of spurious “double ITCZ” problem in CMIP5 coupled models from AMIP simulations. *Geophysical Research Letters*, 44(3), 1520–1527. doi: 10.1002/2016GL071992
- Zhang, B., Zhao, M., & Tan, Z. (2023). Using a Green’s Function Approach to Diagnose

- the Pattern Effect in GFDL AM4 and CM4. *Journal of Climate*, 36(4), 1105 - 1124. doi: 10.1175/JCLI-D-22-0024.1
- Zhao, M., Golaz, J.-C., Held, I. M., Guo, H., Balaji, V., Benson, R., ... Xiang, B. (2018). The GFDL Global Atmosphere and Land Model AM4.0/LM4.0: 1. Simulation Characteristics With Prescribed SSTs. *Journal of Advances in Modeling Earth Systems*, 10(3), 691-734. doi: 10.1002/2017MS001208
- Zheng, X., Tao, C., Zhang, C., Xie, S., Zhang, Y., Xi, B., & Dong, X. (2023). Assessment of CMIP5 and CMIP6 AMIP Simulated Clouds and Surface Shortwave Radiation Using ARM Observations over Different Climate Regions. *Journal of Climate*, 36(24), 8475 - 8495. Retrieved from <https://journals.ametsoc.org/view/journals/clim/36/24/JCLI-D-23-0247.1.xml> doi: 10.1175/JCLI-D-23-0247.1
- Zhou, C., Zelinka, M. D., & Klein, S. A. (2016). Impact of decadal cloud variations on the Earth's energy budget. *Nature Geoscience*, 9(12), 871-874. doi: 10.1038/ngeo2828
- Zhou, C., Zelinka, M. D., & Klein, S. A. (2017). Analyzing the dependence of global cloud feedback on the spatial pattern of sea surface temperature change with a Green's function approach. *Journal of Advances in Modeling Earth Systems*, 9(5), 2174-2189. doi: 10.1002/2017MS001096
- Zhou, L., Lin, S.-J., Chen, J.-H., Harris, L. M., Chen, X., & Rees, S. L. (2019). Toward Convective-Scale Prediction within the Next Generation Global Prediction System. *Bulletin of the American Meteorological Society*, 100(7), 1225 - 1243. doi: 10.1175/BAMS-D-17-0246.1